STREAMLINE-BASED CONCEPTS FOR SPACE-TIME ANALYSIS OF 2D TIME-DEPENDENT FLOW

G.K. KARCH[c], F. SADLO, D. WEISKOPF, T. ERTL

VISUS – Visualization Research Center, University of Stuttgart, Stuttgart, Germany
[c]Corresponding author: Tel.:+4971168588609; Fax: +4971168588620; Email: karchgz@visus.uni-stuttgart.de

KEYWORDS:
> **Main subjects:** space-time visualization, Galilean invariance
> **Fluid:** time-dependent 2D
> **Visualization method(s):** computational visualization
> **Other keywords:** vortex core lines, material lines, line integral convolution

ABSTRACT : *We investigate the application of different streamline-based visualization concepts to the 3D space-time representation of 2D time-dependent flow. This way, we directly obtain from each 3D streamline-based concept a 2D pathline-based counterpart that is Galilean-invariant and takes the time-dependence of the original field explicitly into account. We show the advantages of the overall approach for vortex analysis and the analysis of the dynamics of material lines. In particular, we employ the concept for the extraction of vortex centers, vortex core regions, and the visualization of material line dynamics using streamsurface integration and line integral convolution in the space-time field.*

1   Introduction

Computational visualization is an essential tool for the analysis of flow fields from simulation and measurement. The utilized techniques can be categorized into different classes. Prominent examples are techniques based on integral curves, such as stream-, path-, streak-, and material lines, and feature extraction. While pathlines, streaklines, and material lines are readily applicable to time-dependent flow, the development of feature extraction techniques that take into account the time-dependence of flows is subject to current research.

In this paper, we employ the space-time representation for the visualization of 2D time-dependent vector fields. By treating time as the third dimension of the domain and by extending the original vector by a constant third component equal to one, we obtain a 3D vector field in which streamlines represent pathlines of the original 2D vector field. This represents the analog to making an n-dimensional system of ordinary differential equations autonomous by lifting its dimension to $n + 1$. As a consequence, concepts based on 3D streamlines in the space-time vector field are in fact based on 2D pathlines in the original field, making them Galilean-invariant and time-aware. Galilean invariance is a beneficial, if not mandatory, property of visualization techniques, in particular for the analysis of time-dependent flow and when analyzing flow in configurations where no natural frame of reference is given. Thus, we investigate in this paper the application of existing 3D streamline-based concepts to the space-time representation of 2D time-dependent flow, resulting in techniques for visualization and feature extraction that are Galilean invariant and explicitly take into account the time-dependence of flow fields.

Specifically, our contributions include (1) the introduction and evaluation of space-time normalized helicity, (2) the closely related extraction of vortex core lines according to Levy et al.'s criterion [12], applied

to the space-time field, and (3) material line ribbons constrained to the vicinity of vortex core lines to provide the space-time dynamics within vortices.

2   Related Work

Computational visualization of time-dependent flow by means of integral curves has a long history. While the extraction of individual curves is an established concept, recent strategies concentrate on accurate interactive placement of individual curves [8] and adaptive interactive placement of small sets of curves [15]. Recent research in the field of static sets of trajectories focuses on the efficient computation of their end points or quantities along them [7], and placement strategies for sets of whole trajectories. Research in placement of integral curves was initiated by the image-guided streamline placement due to Turk and Banks [24]. After several works on the placement of streamlines which, e.g., extended the concept to 3D [14] or took into account vector field topology for improved placement [30], there has been recent research on the placement of streamsurfaces [4] in 3D and placement of streaklines and pathlines in 2D flow to avoid intersection and cusps by limiting their length [28], and on the placement of pathlines that avoids intersection of the curves by decoupling integration and visualization scales [6].

Further increase in curve density converges to a result where the entire domain is filled with curves. While uniform coloring of the lines would lead to uniform and, thus, inexpressive visualization, there is a whole field of research, subsumed as texture-based flow visualization, on introducing color that provides properties of (time-dependent) flow. One of the early works in this field is line integral convolution (LIC) [2]. The basic idea of this approach is to convolve a noise texture along streamlines, providing a dense representation of vector fields. In our present work, we employ this technique in the 3D space-time field on surface representations to depict space-time flow behavior. We refer the reader to the survey by Laramee et al. [11] for further details on texture-based flow visualization techniques.

Space-time representation of 2D data was successfully employed in a wide range of time-dependent applications in computational visualization. Examples range from the tracking of critical points in vector fields [23] to the analysis of eye tracking data from video streams [10]. While the space-time representation in visualization often serves a better presentation, there are examples where it also plays a substantial role in the definition of features. One such example, and the work most closely related to ours, is the vortex core line concept by Weinkauf et al. [27] that takes into account the time-dependence of fields.

A further useful property of space-time representation is that 2D time-dependent vector fields can be transformed into steady 3D ones by treating time as additional dimension. In this representation, pathlines, i.e., the true trajectories in the 2D time-dependent flow, represent streamlines, i.e., instantaneous integral curves, in the 3D space-time field. As will be discussed below, streamsurfaces in this 3D field represent streaklines or material lines in the original flow, providing an overall framework and facilitating their extraction.

3   Space-Time Visualization

We start with a short introduction to the space-time representation in Section 3.1. This is followed by a discussion of the different types of characteristic curves and derived constructs, in the context of space-time representation (Section 3.2). Sections 3.3 and 3.4 provide details on our space-time vortex visualization techniques. Finally, we provide a short description of space-time LIC in Section 3.5.

3.1 Space-Time Representation

Given the time-dependent 2D vector field

$$\mathbf{u}(\mathbf{x},t) := \left(\begin{array}{c} u(x,y,t) \\ v(x,y,t) \end{array} \right), \tag{1}$$

with $\mathbf{x} := (x,y)^\top$ and time t, we derive its 3D space-time representation

$$\mathbf{u}'(\mathbf{x}') := \left(\begin{array}{c} u(x,y,t) \\ v(x,y,t) \\ 1 \end{array} \right), \tag{2}$$

with $\mathbf{x}' := (x,y,t)^\top$ by treating the time domain as third spatial axis and by introducing the third vector component equal to one. This ensures that as we step along the vector field $\mathbf{u}'$, we also move the respective amount of time along the time axis, bringing us to the correct time step of the time-dependent vector field. This way, one obtains a stationary 3D vector field that encodes the dynamics of the original time-dependent 2D vector field. Please note that we employ trilinear interpolation of $\mathbf{u}'$ in our tests, i.e., we combine spatial bilinear interpolation with linear interpolation in time. For more details, we refer the reader to related work [27].

3.2 Characteristic Curves

Streamlines of the original (time-dependent) field $\mathbf{u}$ represent instantaneous integral curves. In the space-time framework, they could be obtained by solving initial value problems in the modified representation $(u(x,y,t), v(x,y,t), 0)^\top$. Since the focus of the present work is to account for time-dependence, we do not make use of streamlines in $\mathbf{u}$. Pathlines, in contrast, represent the true time-dependent trajectories in flow fields. Since $\mathbf{u}'$ represents a stationary 3D vector field of the original time-dependent 2D vector field $\mathbf{u}$, 3D streamlines in $\mathbf{u}'$ represent pathlines in $\mathbf{u}$, i.e., when projecting the 3D streamline along the time axis, one obtains the respective pathline in $\mathbf{u}$.

During the last decade, streaklines have been increasingly attracting attention in computational visualization. Streaklines can be seen as a special case of material lines. While material lines consist of any line-type arrangement of massless particles that moves with the flow, streaklines represent curves obtained by continuously releasing particles at a given location, called the seed. In other words, any material line that passes through a fixed seed point over time represents a streakline. It has to be noted that there is a more generic definition of streaklines, the so-called generalized streaklines [29], where the seed is allowed to move over time. This concept accounts for experimental visualizations where the seeding probe is moved while the marker is released, as commonly employed with smoke in wind tunnels. If we allow the point to move infinitely fast, one can generate any connected material line. Streaklines proved particularly useful in recent research on time-dependent vector field topology, where the role of streamlines in the traditional concept has been replaced by streaklines in 2D [20] and streaksurfaces in 3D [26] vector fields.

A streamsurface is obtained by densely seeding streamlines along a seeding curve. Since each particle of a material line moves along a pathline and because all particles move for the same time duration, one can obtain material lines by means of streamsurface integration in $\mathbf{u}'$. All $t = $ const.-sections of these streamsurfaces represent the material line at the respective time. Since material lines are seeded only at

(a) $t = 0.05$ s   (b) $t = 1$ s   (c) $t = 1.5$ s   (d) $t = 2.5$ s   (e) $t \in [0,3]$ s
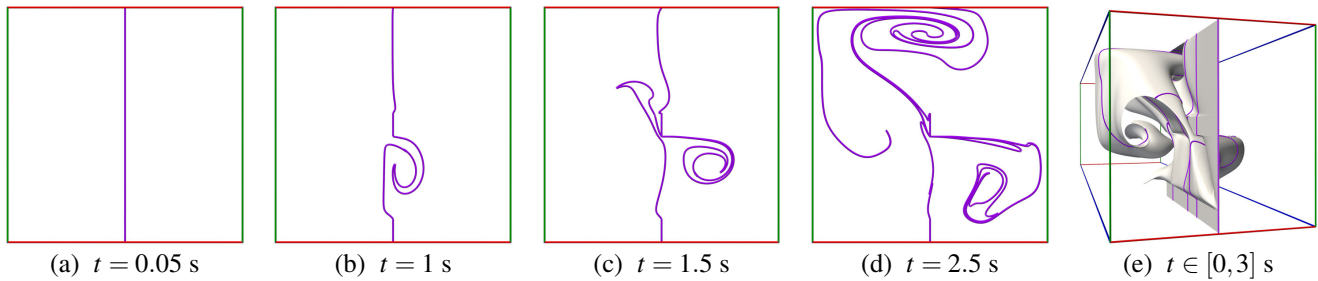
Fig. 1 Material lines and space-time representation. (a) A material line (purple) is seeded as a vertical line at the center of the spatial domain. (b)–(d) The material line folds and stretches continuously in the unsteady flow. (e) $t = const.$-sections of the streamsurface of $\mathbf{u}'$ represent the material lines from (a)–(d).

one instant of time along a curve, the seeding curve of the streamsurface needs to be located in $\mathbf{u}'$ within an xy-plane, i.e., it has no extent in time. Figs. 1(a)–1(d) demonstrate material lines at selected $t = $ const.-instants, which represent sections of the corresponding space-time streamsurface shown in Fig. 1(e). If, on the other hand, the seeding curve for a streamsurface in $\mathbf{u}'$ is a straight line aligned with the time axis, the resulting streamsurface represents a traditional streakline, i.e., each $t = $ const.-section of this surface represents the respective streakline at that instant of time. If the seeding curve is a generic curve in $\mathbf{u}'$ and is monotonically increasing along the time axis, $t = $ const.-sections of this streamsurface represent respective generalized streaklines.

Streamribbons [25] can be seen as a special case between streamlines and streamsurfaces. They represent narrow constant-width strips whose medial axis is a streamline but which additionally show twist. Streamribbons are usually constructed by integrating a streamline and during integration, an initially randomly chosen orientation vector is propagated along the streamline. During this propagation, the direction vector is kept orthogonal to the streamline tangent and rotated based on the velocity gradient, i.e., rotated the way a particle in the vicinity of the streamline would locally rotate around the streamline. From this information, a narrow band is constructed by generating a triangulated surface strip along the streamline with the respective twist. However, using this traditional concept of streamribbons would not be applicable in our space-time context, since streamlines of $\mathbf{u}'$ are monotonically increasing along the time axis t, while the edges of the ribbon would likely move reverse in time due to twist. In other words, while in true 3D vector fields streamribbons typically represent an appropriate approximation of swirling flow behavior, rotation in $\mathbf{u}'$ takes place in the xy-plane only. Hence, streamribbons whose streamline is not aligned with the t-axis, would be subject to inappropriate representation, i.e., the edges of the ribbons could point in reverse time, which would be misleading. Therefore, we propose space-time vortex core ribbons in Section 3.4, a modified concept for visualizing vortical flow in 3D space-time.

3.3 Vortex Core Lines

Vortex core lines represent the axes of vortices in 3D flow, i.e., neighboring particles swirl around these lines. Since there is no general definition of a vortex, there also exists a multitude of definitions for vortex core lines. It has to be noted that although a vortex core line has to be tangent to streamlines in steady flow, it is a common circumstance that vortex core lines do not represent single streamlines. Instead, it is rather the case that a given streamline represents only a short part of a vortex core line and that the successive part of the core line is represented by another streamline [19]. In steady flow, vortex

core lines can be defined locally as those streamlines that exhibit minimum curvature (with the additional requirement of complex eigenvalues of the Jacobian). Sujudi and Haimes [22] define vortex core lines to consist of those points where $\nabla \mathbf{u}$ exhibits a pair of complex eigenvalues and a real eigenvalue λ_R, and where $\mathbf{u}$ is parallel (or antiparallel) to its real eigenvector $\boldsymbol{\varepsilon}_R$, i.e., $(\nabla \mathbf{u})\mathbf{u} = \lambda_R \mathbf{u}$. This requirement is identical to $\mathbf{a} = \lambda_R \mathbf{u}$, i.e., acceleration $\mathbf{a} := (\nabla \mathbf{u})\mathbf{u}$ being (anti)parallel to velocity, which requires the streamline passing through the respective point of the core line to be locally straight. Weinkauf et al. [27] extend this instantaneous approach for 2D and 3D time-dependent flow by applying it to $\mathbf{u}'$ and the 4D space-time representation of 3D time-dependent flow, respectively. This way, they require vortex core lines in time-dependent flow to be tangent to pathlines instead of streamlines. Note that in the case of 2D flow, the vortex core lines in $\mathbf{u}'$ represent a space-time representation of the vortex centers of the 2D flow over time. Weinkauf et al. [27] compare their results to the standard vortex center extraction approach for 2D flow fields, i.e., they also extract critical points of type focus and center [17].

The parallel vectors operator [16] is commonly used for the definition and extraction of line-type features: it identifies points where two vector fields are parallel or antiparallel. In this framework, the angle between the feature tangent, in our case the tangent to the vortex core line, and the two parallel vectors serves as a quality measure, that we denote here as angle criterion. The smaller this angle, the more distinguished the vortex core line is. Nevertheless, in typical cases, one needs to allow quite large, e.g., 45 degrees, angles to avoid disrupted core lines, with the result that there will be parts with flux through the vortex core line. Methods that use the parallel vectors operator, such as the core line definition by Sujudi and Haimes [22], provide accurate results when the core lines are straight, but they are rather inaccurate in regions where the core lines are curved [18]. A recent work [13] on the extraction of bifurcation lines according to Perry and Chong [17] employs refinement of the resulting feature line to avoid this error, but a respective approach for refining vortex core lines is not yet available. Our vortex core line extraction employs the algorithm described by Peikert and Roth [16], where each quad face of a grid cell is split in two triangles to detect the intersection points of the core line with the cell faces.

Another widely used vortex core line criterion, that is also amenable to definition by the parallel vectors operator and denoted as Levy's approach in this paper, is based on the vortex criterion called normalized helicity [12]. Normalized helicity h is a scalar field defined as the normalized dot product of velocity and vorticity, i.e., $h := \mathbf{u} \cdot (\nabla \times \mathbf{u})/(\|\mathbf{u}\| \cdot \|\nabla \times \mathbf{u}\|)$. Vortex regions exhibit large $|h|$, whereas in non-vortical regions, e.g., in shear flow, $|h|$ is small. As described in the thesis of Roth [18], this directly leads to a vortex core line criterion defining those points as part of a core line where $\mathbf{u} \parallel (\nabla \times \mathbf{u})$ (please note that we use the term 'parallel' as a synonym for 'antiparallel' and that we denote it as '$\parallel$'). Another related vortex criterion is λ_2 [9]. It represents the medium eigenvalue of $\mathbf{S} + \boldsymbol{\Omega}$, with $\mathbf{S} := (\nabla \mathbf{u} + (\nabla \mathbf{u})^\top)/2$ being the symmetric part of the Jacobian and $\boldsymbol{\Omega} := (\nabla \mathbf{u} - (\nabla \mathbf{u})^\top)/2$ its antisymmetric part. Vortex regions are indicated by negative values of λ_2.

A further approach for obtaining vortex core line criteria is the extraction of valley lines or ridge lines from scalar vortex indicators. We denote the extraction of valley lines from λ_2 as Sahner's criterion [21]. While in their original implementation, Sahner et al. extract the valley lines by means of the feature flow field [23], we instead use the parallel vectors operator to extract valley lines according to Eberly's definition [3] for height ridges.

In this paper, we propose applying Levy's and Sahner's vortex core line criteria to $\mathbf{u}'$ to obtain time-dependent definitions for vortex centers in time-dependent 2D flow fields. We compare the results to those from the Sujudi-Haimes criterion in space-time [27], and we propose and evaluate the utility of normalized helicity in the space-time field $\mathbf{u}'$. Overall, it turns out in our experiments (Section 4) that

while the Sujudi-Haimes approach tends to be more accurate, it strongly suffers from disrupted core lines in our applications, even for very large angle criteria. In contrast, Levy's and Sahner's criteria in $\mathbf{u}'$ provide core lines that are more coherent, however, at the cost that they are less accurate than those from the Sujudi-Haimes criterion, but still substantially more accurate than vortex center extraction by means of critical points (which is not Galilean-invariant). Regarding vortex criteria, it turns out that normalized helicity can be superior to λ_2 in some examples, but λ_2 can be superior to normalized helicity in others.

3.4 Vortex Core Ribbons

As motivated in Section 3.2, we derive here an approach inspired by streamribbons. Streamribbons are originally constructed along streamlines and show both the shape of the streamline together with twist. Since vortex core lines are close to streamlines (assuming small angle criteria, as discussed in Section 3.3) in 3D flow fields, or in our case to streamlines in $\mathbf{u}'$, we propose constructing ribbons along vortex core lines to visualize swirling flow. This approach could be applied to any 3D flow field by constructing streamribbons along core lines. Note that a traditional streamribbon [25] started at a point of a vortex core line would typically not follow the core line over longer distances because the angle between flow direction and core line tangent is typically non-vanishing, i.e., it is limited by the typically rather large-chosen angle criterion. Hence, we construct the streamribbon along the vortex core line, i.e., we follow the core line instead of a streamline while generating the triangulated strip. Since rotation takes place in $\mathbf{u}'$ only in the xy-plane (Section 3.2), we introduce a modified ribbon construction scheme here for space-time visualization of 2D time-dependent vortical flow.

Instead of initializing a random direction vector and propagating it along the streamline (or core line), as would be done in 3D flow fields, we simultaneously seed two streamlines in $\mathbf{u}'$ at the 'earlier' end of the space-time core line. We simultaneously integrate both streamlines for a small step, i.e., we obtain the new position of the two particles using the fourth-order Runge-Kutta scheme in $\mathbf{u}'$, and apply an xy-translation to the two positions such that their center of gravity gets located on the vortex core line. Subsequently, we adjust the distance between each of the two points and the closest point on the core line to half of the prescribed ribbon width. Using the resulting two points, we construct a triangulated surface patch that connects to the previous front of the ribbon. The whole process is illustrated in Fig. 2 for the construction of one segment of a space-time vortex core ribbon.

There are two main differences between our space-time approach and the original streamribbon construction [25], irrespective if carried out along streamlines, as in the original definition, or along vortex core lines. First, in the traditional approach, the front of a ribbon is kept perpendicular to the streamline (or core line), while in our space-time approach, the front is kept aligned in the xy-plane, because all streamlines advance at the same pace in time (note the 1-component in Equation 2). Hence, the width of our space-time vortex core ribbon is not constant in space-time. Instead, its section with xy-planes has constant length. This has the benefit that the tangents of the ribbon cannot point reverse in time. Second, while the twist of traditional ribbons would express differential rotation at the central streamline (or vortex core line), the twist of our space-time vortex ribbon expresses the combined twist of the two streamlines locally positioned at both sides of the ribbon. This is less misleading, in particular for wide ribbons, because ribbon-based visualization implies that the shape of the ribbon not only shows flow at its medial axis but along its overall extent.
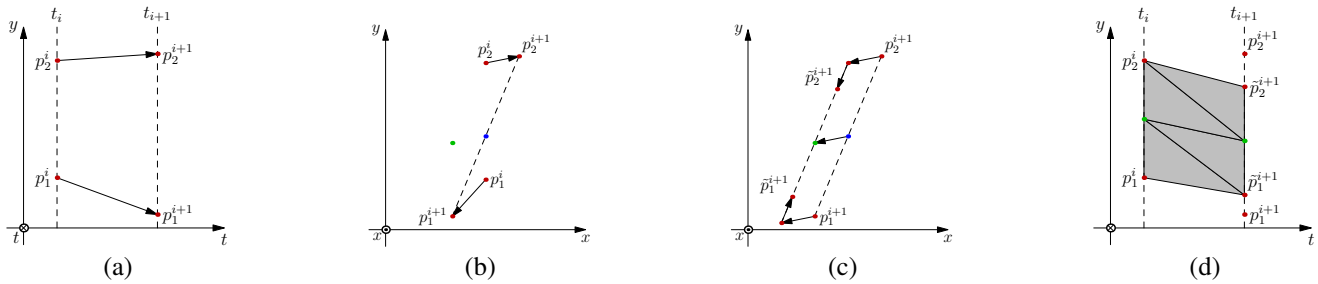
Fig. 2 Construction of space-time vortex core ribbons. (a) Two particles p_1^i and p_2^i (red dots) are seeded at time t_i and integrated forward to t_{i+1}. In (b) the same as in (a) is shown with time axis pointing outside the page. (c) At $t = t_{i+1}$, the particles are translated so that their center of gravity (blue) lies on the vortex core line (green) and the distance between them is equal to the ribbon width (points $\tilde{p}^{i+1}$). (d) Between the points p^i and $\tilde{p}^{i+1}$, a triangle mesh is generated. More triangles per segment can be generated for better texture sampling (see Fig. 7).

3.5 Space-Time Line Integral Convolution

Line integral convolution [2] can be carried out on 2D or 3D domains. It requires two texture buffers: a noise texture and the output texture, both usually represented by uniform grids and of equal extent and resolution. The noise texture is initialized with random values, and, to prevent aliasing in the resulting visualizations, the noise is appropriately blurred with a low-pass filter. Then, at each sample point **p** of the output texture, a forward and a reverse streamline is started with identical user-defined integration time. These two streamlines are combined to a single streamline and used as a convolution filter, i.e., the noise is sampled uniformly along the streamline, weighted by a 1D filter kernel that spans the streamline (usually a box filter or a Gaussian), and integrated. The resulting value is stored in the output texture at the sample point **p**. As a result, the noise gets low-pass filtered ('smeared') along streamlines and thus visualizes the dynamics of the vector field.

In our approach, we employ 3D LIC to the space-time vector field **u**′. Thus, the output texture is a 3D scalar field containing the smeared LIC noise, which we denote as space-time LIC. We map this space-time LIC to surfaces to visualize the space-time dynamics of the vector field at these surfaces, similar to Bachthaler et al. [1]. In cases where a surface region is aligned with **u**′, i.e., locally a streamsurface of **u**′, the resulting pattern on the surface exhibits the shapes of the streamlines used for LIC computation. In cases where the surface region is perpendicular to **u**′, the resulting pattern exhibits rather dots.

4 Results

The utility of our space-time visualization concepts is demonstrated using two 2D time-dependent examples from computational fluid dynamics (CFD): a buoyant flow, and a von Kármán vortex street.

4.1 Buoyant Flow

The first dataset represents a 2D CFD simulation of air flow in a closed container with two obstacles, which make the flow more unsteady. The bottom wall is heated at $75°C$ and the upper wall is cooled to $5°C$. This drives a buoyant convection flow. The side walls exhibit adiabatic boundary condition and all walls are no-slip boundaries. The data is given on a block-structured grid with an overall resolution of
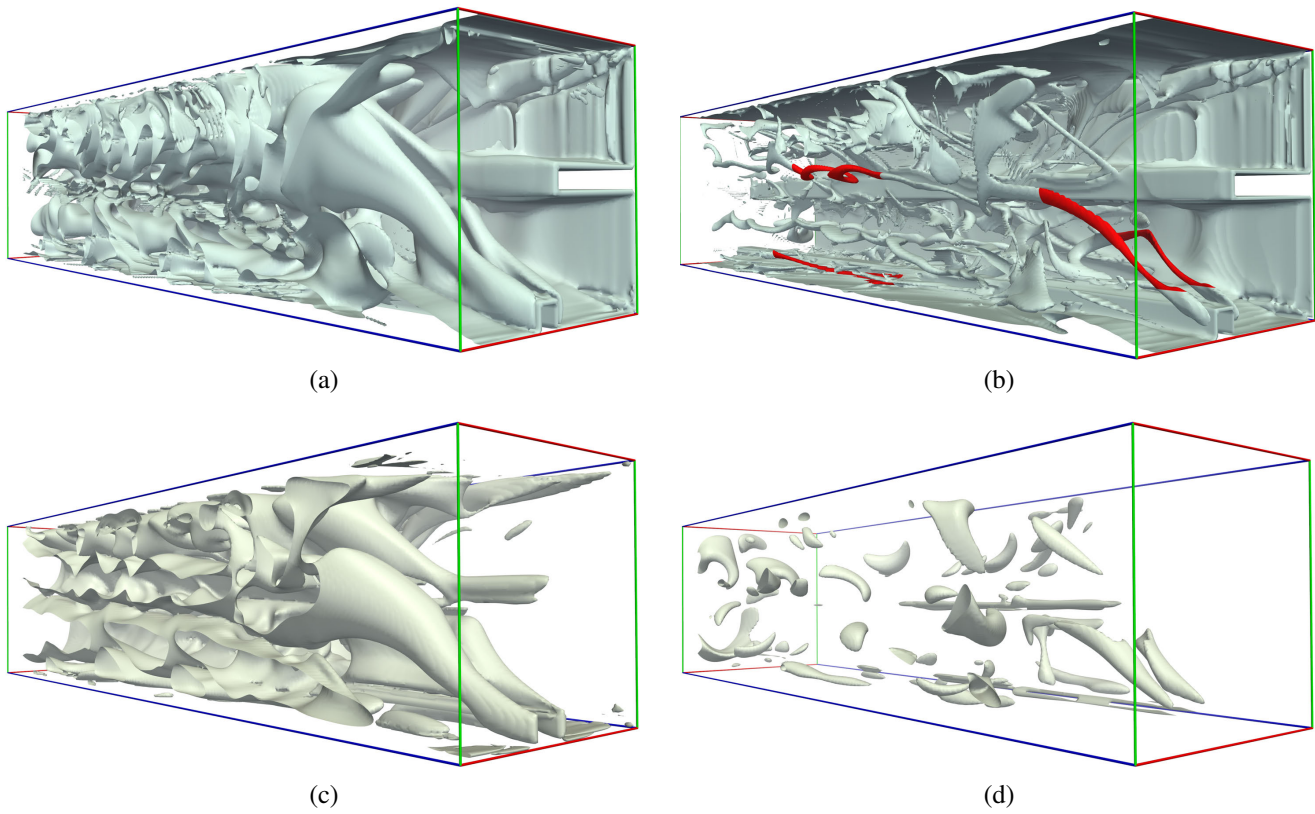
Fig. 3 Buoyant Flow dataset in space-time representation (x: red, y: green, t: blue), with time increasing to the left. (a) Isosurface of normalized helicity of $\mathbf{u}'$ at isolevel 0.6 provides rather cluttered visualization. (b) Same as (a), but isolevel 0.95 nicely reveals individual vortices over time. Regions marked in red are visualized in Figs. 5(a) and 5(b). (c) Isosurface of λ_2 of $\mathbf{u}'$ at isolevel -0.0001 results in clutter, similar to (a). (d) Same as (c), but, compared to (b), isolevel -70.0 fails at revealing dynamics of the vortices.

101×101 nodes and 401 time steps.

In Fig. 3, we provide visualizations by means of isosurfaces of vortex criteria. Figs. 3(a) and (b) show isosurfaces of normalized helicity of $\mathbf{u}'$, at isolevels 0.6 and 0.95, respectively. Note that the isosurface was clipped at the x-max face of the domain to provide view to the inside. In Fig. 3(b), one can see how two vortices originate at the bottom square obstacle and start to rise (two red parts on the right hand side of the figure). Normalized helicity provides results superior to λ_2 (Figs. 3(c) and (d)) in this dataset.

Next, we investigate different vortex core line definitions using the same dataset (Fig. 4). In this dataset, critical points, Sujudi-Haimes core lines, and Levy core lines provide comparable results while valley lines of λ_2 somewhat deviate. It is apparent that the Sujudi-Haimes core lines are severely disrupted and it is difficult to discern the vortical structure. On the other hand, our space-time Levy criterion clearly reveals the vortex structure in the unsteady flow. Fig. 5 provides a more detailed comparison. In Fig. 5(a), pathlines seeded at Sujudi-Haimes core lines (yellow) exhibit least swirl, i.e., they follow the yellow core line tightly, while pathlines started at Levy core lines (blue) exhibit more swirl. Pathlines started at critical points (red) exhibit even more swirl, while pathlines seeded at λ_2 valley cores (green) exhibit the largest swirl radius and are therefore most inaccurate. Hence, Sujudi-Haimes core lines are most accurate
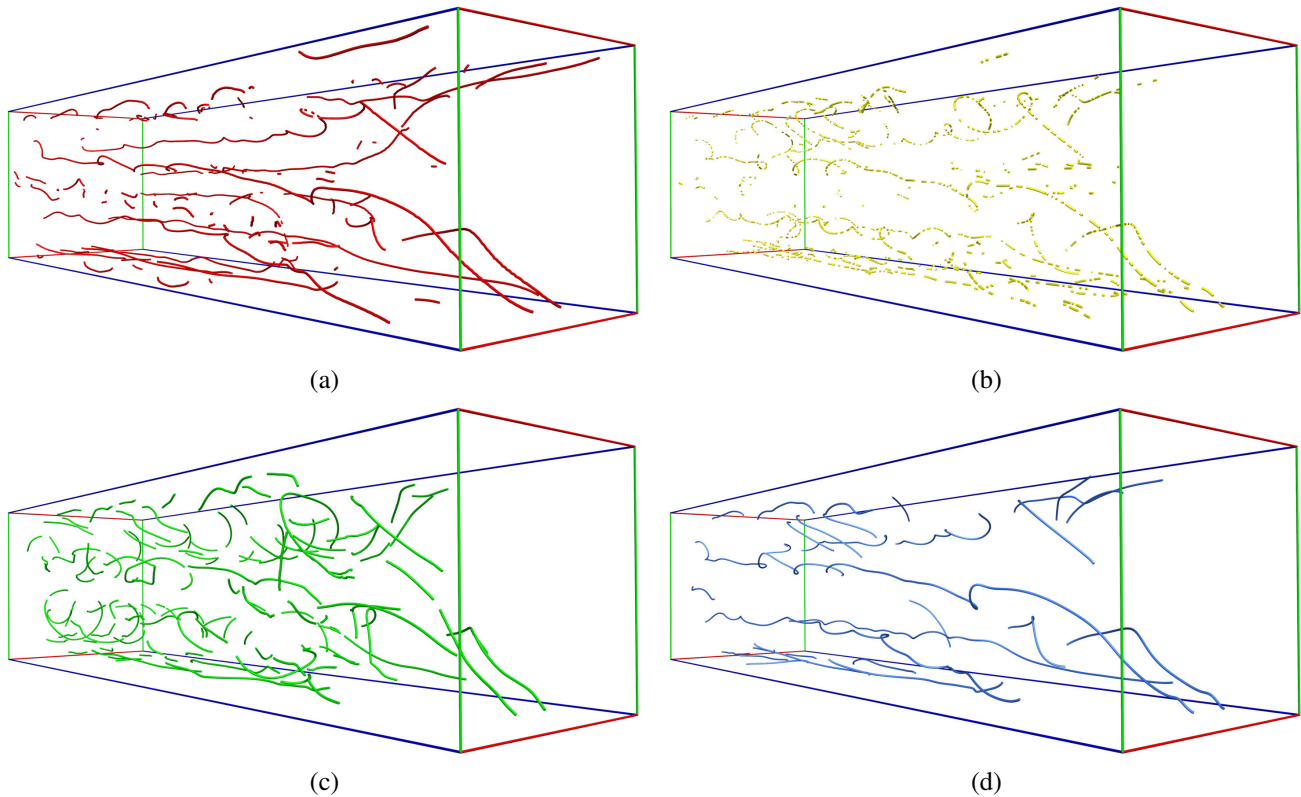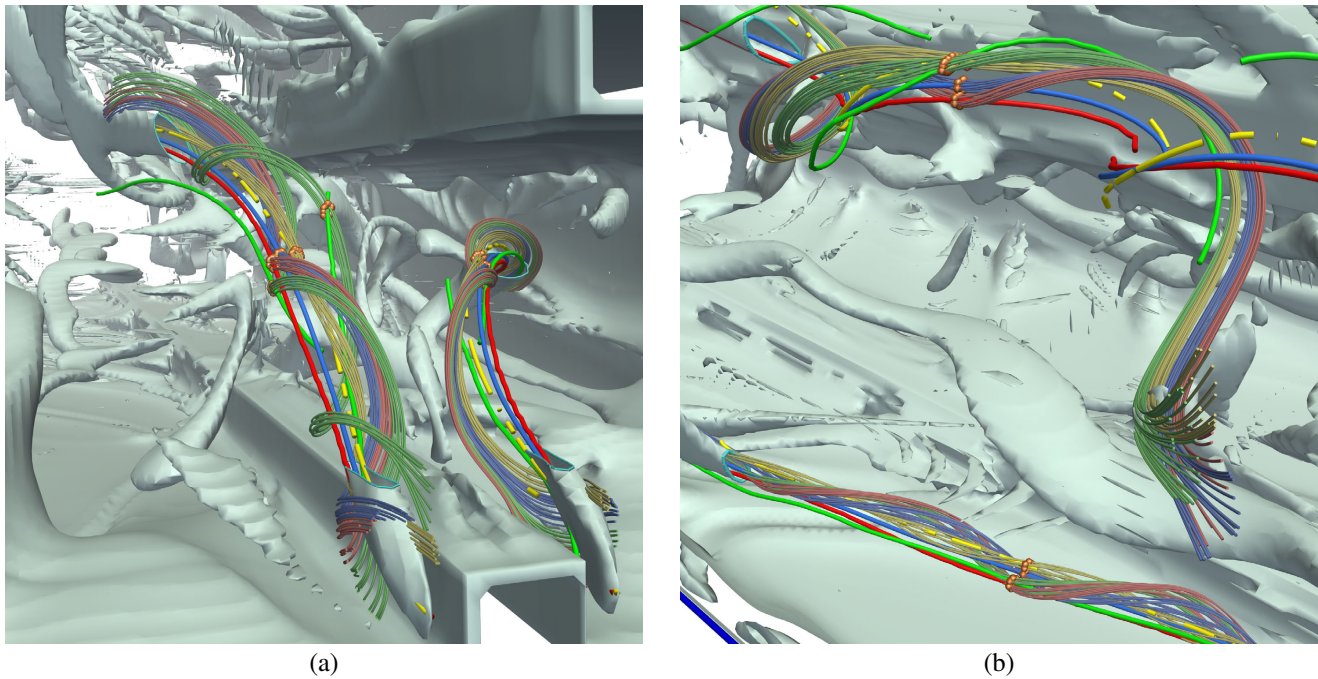
Fig. 4 Space-time vortex core lines in Buoyant Flow dataset. Time again increases from right to left. (a) Space-time curves of critical points of type focus and center in **u**. (b) Sujudi-Haimes vortex core lines in **u**′ are severely disrupted. (c) λ_2 valley lines in **u**′. (d) Levy vortex core lines in **u**′. Please see Fig. 5 for a detailed comparison.

in this dataset, however, with the drawback that they are strongly disrupted. This affects perception and can hinder derived visualization, e.g., the construction of our vortex core ribbons (Fig. 7(c)). In Fig. 5(b), one can see that pathlines seeded at the Sujudi-Haimes core line at the upper curved vortex are again closest to the vortex center. On the other hand, all definitions provide similar results at the vortex at the bottom of Fig. 5(b), because this vortex is straight and oriented along the t-axis, i.e., the vortex does not move within the examined time interval. All in all, we obtained best results with the space-time Levy criterion, as it provides a good tradeoff between accuracy and readability—although it deviates from the true vortex core more than Sujudi-Haimes criterion, it provides more continuous structure and it is more accurate than vortex visualization by means of critical points or valley lines of λ_2 in **u**′.

Fig. 6 demonstrates the use of space-time LIC on streamsurfaces of **u**′, i.e., on material lines in space-time representation. Due to the LIC, one can easily interpret the dynamics within the material line. The ridges in a slice of the finite-time Lyapunov exponent (FTLE) field [5], which is computed from trajectories started at the FTLE slice in space-time and integrated in reverse time until the start of the dataset, exhibit high correlation with the material line because the material line is attracted by the ridges in the FTLE field, which represent attracting Lagrangian coherent structures (LCS). In streakline-based vector field topology [20], streaklines seeded along hyperbolic trajectories extract all attracting and repelling LCS. Since in our case, we seeded a material line at the purple curve instead, there are some deviations between

Fig. 5 Selected vortex regions in Buoyant Flow dataset, vortex core lines by saturated tubes (colors from Fig. 4), with pathlines by low-saturated thin tubes, seeded at the orange spheres at the respective core line, and isosurface of normalized helicity for context. (a) Visualization of the region depicted in red at the right side of Fig. 3(b). (b) Red region at the left side of Fig. 3(b), same visualization as in (a).

the FTLE ridges and the material line. Our space-time material lines give insight into topology-related flow behavior, without costly computations as would be required to obtain the FTLE field.

Finally, we demonstrate in Fig. 7 the utility of our vortex core ribbons. While narrow ribbons reduce occlusion and better visualize twist along the core lines, they are too narrow to appropriately visualize the LIC texture. Increased ribbon width shows LIC texture well. One can identify regions where the LIC patterns cross the core line or where the patterns are more point-like than line-like. These are locations along the core line where the flow does not exhibit distinct vortical motion. Hence, with the presented method, one can investigate the flow around extracted core lines with respect to vortical motion. Finally, although the Sujudi-Haimes criterion provides more accurate results, the frequent disruption of core lines leads to disintegrated and inferior vortex core ribbons which are very hard to interpret. This motivates the use of our proposed space-time Levy core line criterion also for vortex ribbons in this dataset.

4.2 von Kármán Vortex Street

The second dataset comes from a simulation of a fluid flow with a quadrangular obstacle at the upstream end, resulting in vortex shedding. The dataset has a resolution of 101×301 nodes and 801 time steps and, similarly to the first dataset, is represented on a block-structured grid.

The isosurfaces of normalized helicity and λ_2 in Figs. 8(a) and (b), respectively, show the space-time structure of the vortices. The vortices detach from the obstacle and move upwards with the overall flow. In this dataset, the space-time λ_2 isosurface is superior to the one extracted from space-time normalized

(a)

(b)

(c)

(d)
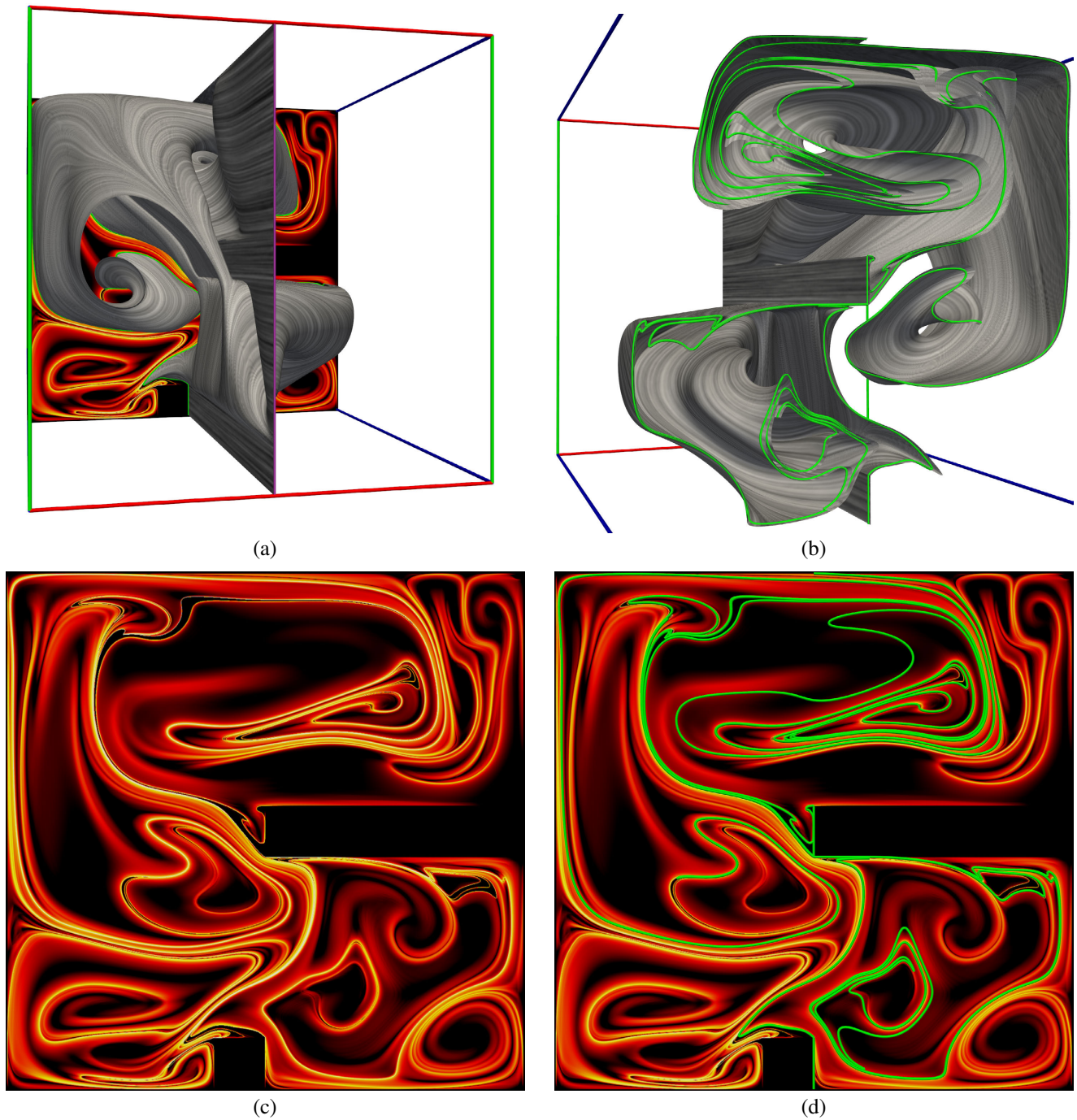
Fig. 6 (a) Space-time material line in Buoyant Flow dataset, seeded at purple curve, with space-time LIC visualizing stretching and folding of material line. Material line stretching is apparent, e.g., from the LIC at the top left region. The FTLE field located at the respective instant in time exhibits high correlation with the material line (green intersection curve in (b)). The FTLE field (c), and both the material line and the FTLE field for comparison (d).
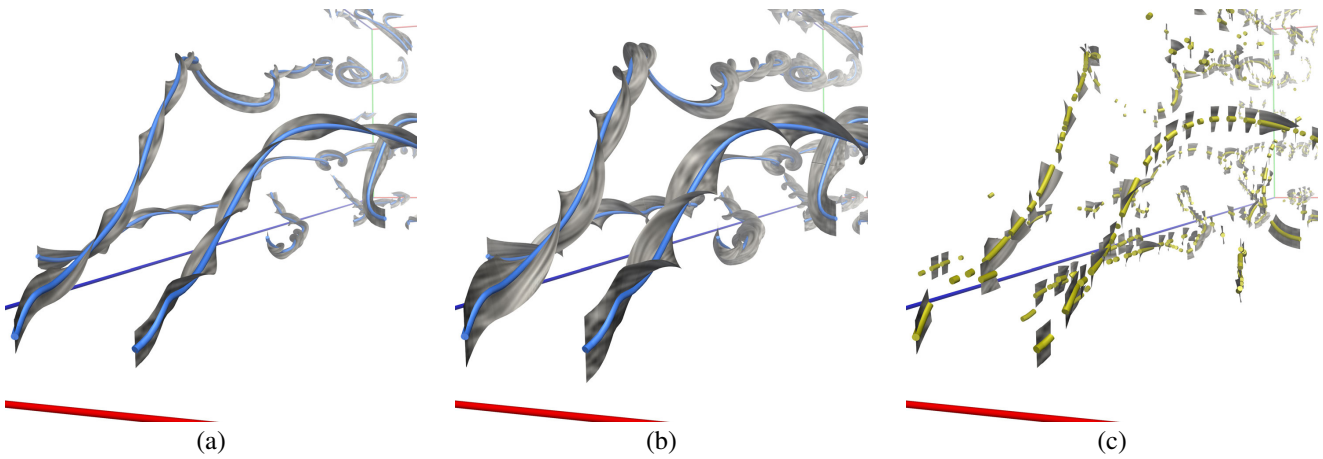
Fig. 7 Space-time vortex core ribbons textured with space-time LIC in Buoyant Flow dataset, with focus on region from Fig. 5(a). (a) Narrow vortex core ribbons along Levy core lines in $\mathbf{u}'$ nicely visualize twist along core line, i.e., the rotational behavior of the vortices. However, the bands are too narrow to visualize the LIC texture well. (b) Same as (a), but with wider ribbons to better show space-time LIC texture. (c) Same as (a), but applied to Sujudi-Haimes core lines suffers from their disrupted geometry, resulting in visual clutter.
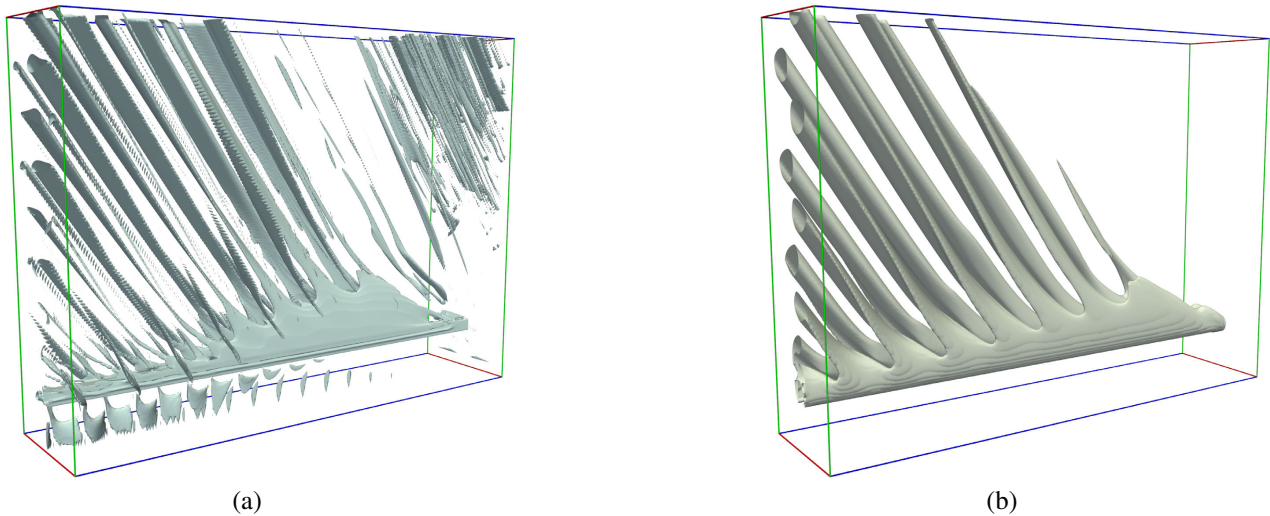
Fig. 8 von Kármán Vortex Street dataset in space-time representation (time increasing to the left). (a) Isosurface of normalized space-time helicity at isolevel 0.98, and (b) isosurface of space-time λ_2 at isolevel -1000. Both criteria reveal upward motion of vortices, however, (a) suffers more from numerical issues.

helicity, since the vortical structure is more pronounced and not cluttered by noise. The λ_2 isosurface boundary at the last time step (left side) additionally reveals that the vortex regions grow over time, since the 'tubes' representing older vortices are larger, as can be seen at the top of the space-time boundary. In Figs. 9(a) and (b), vortex core lines are shown with the same color scheme as in the Buoyant Flow dataset. There are no critical points representing vortical flow due to the fast motion of the vortices.

(b)
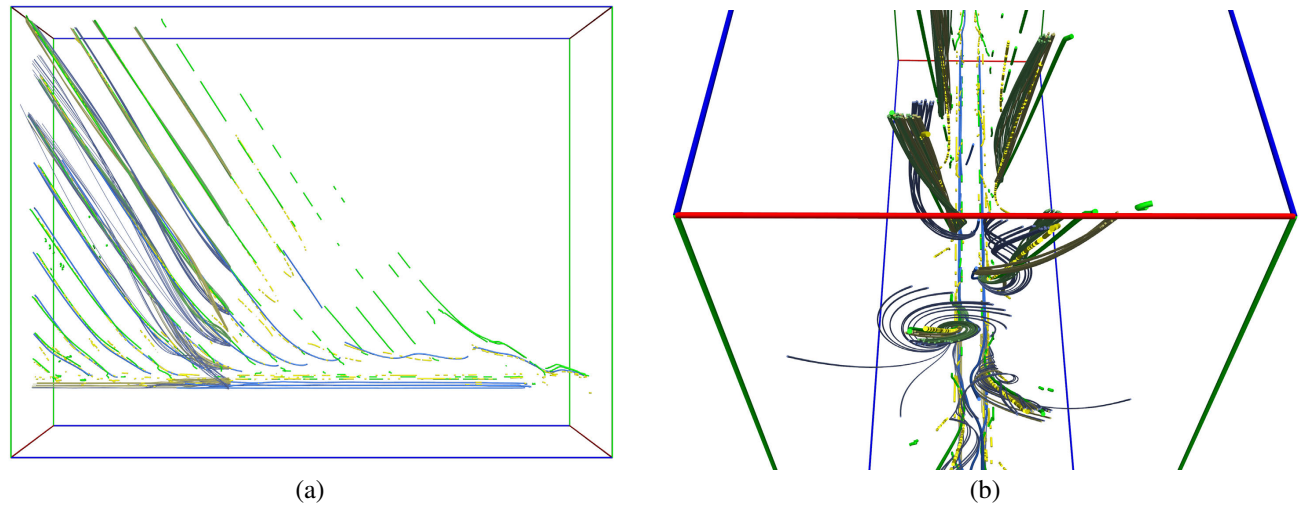
Fig. 9 Space-time vortex core lines with seeded pathlines in von Kármán Vortex Street dataset. (a),(b) space-time λ_2 valley lines are closer to Sujudi-Haimes core lines, while core lines according to Levy deviate. Pathlines swirl around Sujudi-Haimes core lines, indicating their superior quality.

Fig. 9(a) shows an overview of the dataset. Here, the upward motion of the vortices is well captured by the vortex core lines. It is apparent that the vortices are well developed only after roughly half of the time domain. The pathlines seeded close to the obstacle are more chaotic and tend to 'jump' between core lines. The ones seeded in the upper part are more stable, and are attracted toward the Sujudi-Haimes vortex core lines, as visible in Fig. 9(b). On the other hand, the Levy's vortex core lines nicely show the detachment of the vortices from the obstacle, and result in more continuous curves that are better readable than the disrupted cores based on the Sujudi-Haimes criterion. The Levy's cores are, however, moving toward the center, between the Sujudi-Haimes cores. The valley lines of space-time λ_2, in contrast, are close to the Sujudi-Haimes cores and represent a preferable choice in this dataset.

5   Conclusion

We presented different visualization techniques for 2D time-dependent vector fields. Transforming the original field into 3D space-time representation allows us to employ techniques that are based on 3D streamlines. Since streamlines in this field represent pathlines in the original 2D field, the resulting visualizations are Galilean invariant and explicitly take into account the time-dependence of the original vector field. In our experiments, we observed difficulties with the Sujudi-Haimes vortex core line criterion, which has already been applied in space-time before [27]. As an alternative, we employed vortex core line extraction according to Levy et al. and Sahner et al. to the space-time representation, which provided less accurate but more consistent results leading to a preferable tradeoff. For the visualization of vortical flow in general, and in particular vortices in the 3D space-time field, we introduced vortex core ribbons. They readily visualize the twist in vortices and by mapping space-time LIC on their manifolds, they provide a notion of vortex core line quality. Beyond this, we employed space-time normalized helicity for visualizing the extent of vortices and also used space-time LIC on space-time streamsurfaces to visualize both extrinsic and intrinsic dynamics of material lines. As future work, we plan to investigate more visualization techniques based on 4D space-time representation of 3D time-dependent vector fields.

Acknowledgments

References

1. Bachthaler S, Sadlo F, Dachsbacher C and Weiskopf D. Space-time visualization of dynamics in Lagrangian coherent structures of time-dependent 2D vector fields. *Proc International Conference on Information Visualization Theory and Applications*. Rome, Italy, pp 573–583, 2012.

2. Cabral B and Leedom LC. Imaging vector fields using line integral convolution. *Proc ACM SIGGRAPH Computer Graphics and Interactive Techniques*. Anaheim, CA, USA, pp 263–270, 1993.

3. Eberly D. *Ridges in Image and Data Analysis*. Kluwer Academic Publishers.

4. Esturo JM, Schulze M, Rössl C and Theisel H. Global selection of stream surfaces. *Computer Graphics Forum*, Vol. 32, No. 2, pp 113–122, 2013.

5. Haller G. Distinguished material surfaces and coherent structures in three-dimensional fluid flows. *Physica D*, Vol. 149, No. 4, pp 248–277, 2001.

6. Hlawatsch M, Sadlo F, Hajun J and Weiskopf D. Pathline glyphs. *Computer Graphics Forum*, Vol. 33, No. 2. to appear, 2014.

7. Hlawatsch M, Sadlo F and Weiskopf D. Hierarchical line integration. *IEEE Transactions on Visualization and Computer Graphics*, Vol. 17, No. 8, pp 1148–1163, 2011.

8. Hlawatsch M, Sadlo F and Weiskopf D. Predictability-based adaptive mouse interaction and zooming for visual flow exploration. *International Journal for Uncertainty Quantification*, Vol. 3, No. 3, pp 225–240, 2013.

9. Jeong J and Hussain F. On the identification of a vortex. *Journal of Fluid Mechanics*, Vol. 285, No. 69, pp 69–94, 1995.

10. Kurzhals K and Weiskopf D. Space-time visual analytics of eye-tracking data for dynamic stimuli. *IEEE Transactions on Visualization and Computer Graphics*, Vol. 12, No. 19, pp 2129–2138, 2013.

11. Laramee RS, Hauser H, Doleisch H, Vrolijk B, Post FH and Weiskopf D. The state of the art in flow visualization: dense and texture-based techniques. *Computer Graphics Forum*, Vol. 23, No. 2, pp 203–221, 2004.

12. Levy Y, Degani D and Seginer A. Graphical visualization of vortical flows by means of helicity. *AIAA*, Vol. 28, No. 8, pp 1347–1352, 1990.

13. Machado G, Sadlo F and Ertl T. Local extraction of bifurcation lines. *Proc Vision, Modelling and Visualization*. Lugano, Switzerland, pp 9–16, 2013.

14. Mattausch O, Theußl T, Hauser H and Gröller E. Strategies for interactive exploration of 3D flow using evenly-spaced illuminated streamlines. *Proc 19th Spring Conference on Computer Graphics*. Budmerice, Slovakia, pp 213–222, 2003.

15. McLoughlin T, Jones M, Laramee R, Malki R, Masters I and Hansen C. Similarity measures for enhancing interactive streamline seeding. *IEEE Transactions on Visualization and Computer Graphics*, Vol. 19, No. 8, pp 1342–1353, 2013.

16. Peikert R and Roth M. The 'parallel vectors' operator – a vector field visualization primitive. *Proc IEEE Visualization*. San Francisco, CA, USA, pp 263–270, 1999.

17. Perry AE and Chong MS. A description of eddying motions and flow patterns using critical-point concepts. *Annual Review of Fluid Mechanics*, Vol. 19, pp 125–155, 1987.

18. Roth M. "Automatic extraction of vortex core lines and other line-type features for scientific visualization". PhD thesis. ETH Zurich, No. 13673, 2000.

19. Sadlo F, Peikert R and Parkinson E. Vorticity based flow analysis and visualization for Pelton turbine design optimization. *Proc IEEE Visualization*. Austin, TX, USA, pp 179–186, 2004.

20. Sadlo F and Weiskopf D. Time-dependent 2-D vector field topology: an approach inspired by Lagrangian coherent structures. *Computer Graphics Forum*, Vol. 29, No. 1, pp 88–100, 2010.

21. Sahner J, Weinkauf T and Hege HC. Galilean invariant extraction and iconic representation of vortex core lines. *Proc Eurographics/IEEE VGTC Symposium on Visualization*. Leeds, United Kingdom, pp 151–160, 2005.

22. Sujudi D and Haimes R. Identification of swirling flow in 3D vector fields. *Proc 12th AIAA Computational Fluid Dynamics Conference*. San Diego, CA, USA, pp 95–1715, 1995.

23. Theisel H and Seidel HP. Feature flow fields. *Proc Eurographics/IEEE VGTC Symposium on Visualization*. Grenoble, France, pp 141–148, 2003.

24. Turk G and Banks D. Image-guided streamline placement. *Proc ACM SIGGRAPH Computer Graphics and Interactive Techniques*. New Orleans, Louisiana, USA, pp 453–460, 1996.

25. Ueng SK, Sikorski C and Ma KL. Efficient streamline, streamribbon, and streamtube constructions on unstructured grids. *IEEE Transactions on Visualization and Computer Graphics*, Vol. 2, No. 2, pp 100–110, 1996.

26. Üffinger M, Sadlo F and Ertl T. A time-dependent vector field topology based on streak surfaces. *IEEE Transactions on Visualization and Computer Graphics*, Vol. 19, No. 3, pp 379–392, 2013.

27. Weinkauf T, Sahner J, Theisel H and Hege HC. Cores of swirling particle motion in unsteady flows. *IEEE Transactions on Visualization and Computer Graphics*, Vol. 13, No. 6, pp 1759–1766, 2007.

28. Weinkauf T, Theisel H and Sorkine O. Cusps of characteristic curves and intersection-aware visualization of path and streak lines. *Topological Methods in Data Analysis and Visualization II*. Springer, pp 161–176, 2012.

29. Wiebel A, Tricoche X, Schneider D, Jänicke H and Scheuermann G. Generalized streak lines: analysis and visualization of boundary induced vortices. *IEEE Transactions on Visualization and Computer Graphics*, Vol. 13, No. 6, pp 1735–1742, 2007.

30. Ye X, Kao D and Pang A. Strategy for scalable seeding of 3D streamlines. *Proc IEEE Visualization*. Minneapolis, Minnesota, USA, pp 471–478, 2005.

Copyright Statement